Biochimica et Biophysica Acta 1858 (2016) 75–84

Contents lists available at ScienceDirect

Biochimica et Biophysica Acta

journal homepage: www.elsevier.com/locate/bbamem

In situ and real time investigation of the evolution of a *Pseudomonas fluorescens* nascent biofilm in the presence of an antimicrobial peptide

Fabienne Quilès [a,b,*], Souhir Saadi [a,b,c], Grégory Francius [a,b], Jalal Bacharouche [a,b], François Humbert [a,b]

[a] **CNRS**, Laboratoire de Chimie Physique et Microbiologie pour l'Environnement, LCPME, UMR 7564, Villers-lès-Nancy, F-54600, France
[b] Université de Lorraine, Laboratoire de Chimie Physique et Microbiologie pour l'Environnement, LCPME, UMR 7564, Villers-lès-Nancy, F-54600, France
[c] Laboratoire de Biochimie Faculté de Médecine de Sousse, Avenue Mohamed Karoui, 4002 Sousse, Tunisia

ARTICLE INFO

Article history:
Received 26 June 2015
Received in revised form 29 September 2015
Accepted 21 October 2015
Available online 23 October 2015

Keywords:
Bacterial biofilm
Antimicrobial peptide
ATR–FTIR spectroscopy
AFM
Fluorescence images

ABSTRACT

Against the increase of bacterial resistance to traditional antibiotics, antimicrobial peptides (AMP) are considered as promising alternatives. Bacterial biofilms are more resistant to antibiotics that their planktonic counterpart. The purpose of this study was to investigate the action of an AMP against a nascent bacterial biofilm. The activity of dermaseptin S4 derivative S4(1–16)M4Ka against 6 h-old *Pseudomonas fluorescens* biofilms was assessed by using a combination of Attenuated Total Reflectance–Fourier Transform InfraRed (ATR–FTIR) spectroscopy *in situ* and in real time, fluorescence microscopy using the *Bac*light™ kit, and Atomic Force Microscopy (AFM, imaging and force spectroscopy). After exposure to the peptide at three concentrations, different dramatic and fast changes over time were observed in the ATR–FTIR fingerprints reflecting a concentration-dependent action of the AMP. The ATR–FTIR spectra revealed major biochemical and physiological changes, adsorption/accumulation of the AMP on the bacteria, loss of membrane lipids, bacterial detachment, bacterial regrowth, or inhibition of biofilm growth. AFM allowed estimating at the nanoscale the effect of the AMP on the nanomechanical properties of the sessile bacteria. The bacterial membrane elasticity data measured by force spectroscopy were consistent with ATR–FTIR spectra, and they allowed suggesting a mechanism of action of this AMP on sessile *P. fluorescens*. The combination of these three techniques is a powerful tool for *in situ* and in real time monitoring the activity of AMPs against bacteria in a biofilm.

1. Introduction

Biofilms are complex assemblages of microorganisms embedded in a self-produced exopolymer matrix attached to material surfaces [1]. Formation of biofilms is a major economic and health problem in numerous areas from food production to medical implants or water distribution systems. Compared with the planktonic counterparts, the bacteria present in a biofilm can tolerate up to 1000 times more disinfectant or antibiotic [2,3]. Bacteria growing in a biofilm are physiologically distinct from planktonic cells of the same bacteria. The reduced biocide susceptibility of bacteria in biofilms is primarily a function of biofilm structure and composition (delayed penetration of the antimicrobial), but may also be influenced by the physiologic state of bacteria within the biofilm (alteration of the cellular growth rate), adaptive responses (repression or induction of genes), occurrence of persisters even in young biofilms [4,5]. Consequently, their eradication requires higher antibiotic concentrations which unfortunately favour the emergence of multi-resistant strains. Antimicrobial peptides (AMPs) are considered as an alternative to conventional antibiotics since they are not specific, and they are less susceptible to give bacterial resistance [6–8]. Several mechanisms of action are proposed in the literature. The peptides can act by membrane permeabilization and/or as metabolic inhibitors [9,10].

Among the hundreds of antimicrobial peptides discovered, dermaseptin S4, an antimicrobial peptide expressed in amphibian skin, showed a broad antimicrobial activity [11]. It is a linear cationic peptide, which is structured in α-helix in apolar solvents [12]. However, this natural antimicrobial peptide having high antimicrobial effects is also toxic [13–16]. The modification of dermaseptin S4 was therefore performed in order to increase its antimicrobial effects and decrease its toxicity [15,17]. Notably, shorter derivatives have shown to keep a very good antimicrobial activity with a significant decrease of their toxicity [14–16].

The studies of the activity of antimicrobial peptides against bacterial biofilms are quite recent. They deal principally with the inhibition of the formation of a bacterial biofilm analysed after a definite number of hours of the AMP action by usual methods of microbiology, and sometimes microscopy [18–28]. They conclude to the inhibition of the formation of the biofilm often by the analysis of fluorescence or scanning electron microscopy images recorded at the end of the experiments.

These studies gave a picture of the biofilm after several hours of action of the antimicrobial agent. A better understanding of biocide action

* Corresponding author at: CNRS, Laboratoire de Chimie Physique et Microbiologie pour l'Environnement, LCPME, UMR 7564, Villers-lès-Nancy, F-54600, France.
E-mail address: fabienne.quiles@univ-lorraine.fr (F. Quilès).

http://dx.doi.org/10.1016/j.bbamem.2015.10.015
0005-2736/

can only be possible by gaining more insight into their molecular mechanisms of action against sessile bacteria inside the biofilms. Such a goal is possible by probing and tracking *in situ*, at the cellular and/or molecular scales, and in real time the changes induced by AMPs in bacterial cells. Vibrational spectroscopies can be used for such a purpose [29–32]. Among the possible tools, the Attenuated Total Reflectance–Fourier Transform InfraRed (ATR–FTIR) spectroscopy could be a valuable tool. Indeed, because its depth of analysis is typically of the order of 1–2 μm, the ATR–FTIR technique enables, *via* the ATR–FTIR fingerprints of biomolecules, to monitor *in situ* not only the initial stages of biofilm formation but also, subsequently, the response of the base sessile bacteria monolayer to environmental condition changes. It has been successfully employed to explore biofilm formation and biocide transport at solid–liquid interfaces at the molecular scale [33–38]. Furthermore, Atomic Force Microscopy (AFM) is a very attractive tool for studying many biological applications [39–41], such as molecular recognition [42], proteins/proteins interactions, cell/proteins interactions [43], and many other largely intermolecular forces governed phenomena. The ability to detect very low forces (~10 pN) and the high lateral resolution (<10 Å), along the ability to operate in real time [44] under aqueous or physiological conditions [45,46] with minimal sample preparation [47], makes it a good technique for studying biological systems [48]. In addition to its ubiquitous role in the investigation to observe morphological changes induced by the action of an antimicrobial peptide as it was performed on planktonic bacteria [49–51], the AFM can be exploited to probe *in situ* the nanomechanical properties (Young modulus) of the bacterial cells upon action of an antimicrobial peptide [52,53].

The aim of this work was to assess the potential of this physicochemical approach to *in situ* and in real time monitor the changes induced by one antimicrobial peptide in sessile bacterial cells over the early stages of biofilm formation. For this assessment, we have chosen to probe *in situ* the activity of dermaseptin S4 derivative S4(1–16)M4Ka against a 6 h-old *Pseudomonas fluorescens* biofilm. This peptide has shown a high antibacterial activity with a low toxicity [15]. We show here how ATR–FTIR can monitor the interaction of an AMP with sessile bacteria in a young biofilm, *in situ* and in real time. In addition, the bacterial membrane integrity was assayed by the *Bac*light™ kit and AFM was used to visualize the local effect of the antimicrobial peptide upon the cell morphology and nanomechanic properties.

2. Materials and methods

2.1. Antimicrobial peptide

S4(1–16)M4Ka is a cationic peptide modified from dermaseptin S4. Its amino acid sequence is ALWKTLLKKVLKAAAK-NH_2 [15], and its net charge is +6 [54]. It was obtained by stepwise solid phase synthesis using Fmoc (fluoren-9-ylmethoxycarbonyl) polyamide-active ester chemistry as described in a previous work [15]. The peptide was stored at −20 °C as a stock solution at 1 g/L in non-pyrogenic sterile water (Aqua B-Braun, Melsungen, Germany).

2.2. Bacterial strain and culture conditions

The non-pathogenic strain *Pseudomonas fluorescens* CIP 69.13 (batch 1046), a Gram-negative bacterium, was purchased from the collection of the Pasteur Institute (Paris, France). The subculture and culture conditions were the same as in the work of Quilès *et al.* [34]. Briefly, the bacterial subculture was carried out in 400 mL of Lysogeny Broth (LB; Fluka) in deionized water (Millipore Corp., Milli-Q) at 28 ± 1 °C, and under magnetic stirring (300 rpm) for 24 h. 45 mL of the subculture was then introduced in 400 mL fresh sterile LB medium and incubated for 14 h under magnetic stirring. The bacterial growth was monitored by the measurement of the optical density at 620 nm (OD_{620}) with a WPA S1000 Spectrawave visible spectrophotometer (Biochrom Ltd.). The reference was the sterile nutritive medium in which the bacteria were in suspension. The 14 h-old *P. fluorescens* culture, in end-exponential phase, was then harvested by centrifugation (10,000 g, 10 min, and 4 °C) for further use.

2.3. Antimicrobial activity against planktonic P. fluorescens

The antimicrobial assays against planktonic *P. fluorescens* were performed in sterile 96-well plates (Nunc) in a final volume of 100 μL. It was carried out with a modified method from Zairi *et al.* [15]. 20 μl of the stock solution of the peptide was spotted in the fourth plate column wells in presence of 80 μl of non-pyrogenic sterile water, and then a serial of two fold dilutions of the initial concentration was performed and subsequently double diluted in non-pyrogenic sterile water. The centrifugation cap of *P. fluorescens* at end-exponential phase was re-suspended in 200 mL of diluted 1:50 sterile LB medium (0.5 g/L, hereafter called LB/50), adjusted to $OD_{620} = 0.28$ ($\approx 10^8$ CFU/mL). Aliquots (50 μL) of a suspension containing the bacteria in LB/50 were added to 50 μL of the solution containing the peptide in serial 2-fold dilutions. The peptide solution was then serially double diluted from the first well to the next and so forth with non-pyrogenic sterile water (concentration range of 100–1.56 mg/L). The 50 μL peptide solutions were then inoculated with 50 μL of the bacterial suspension previously prepared in LB/50. Sterility and growth controls were 1:100 diluted LB (hereafter called LB/100) and non-pyrogenic sterile water, and a bacterial suspension without peptide, respectively. The plate was incubated for 24 h at 28 °C. The growth of bacteria was determined by means of the occurrence or not of a bacterial cap in the well bottom. Minimal inhibitory concentrations (MICs) were defined as the lowest concentration at which no growth was apparently detectable. MIC was determined from two independent experiments performed in duplicate.

2.4. Biofilm for antibacterial tests

Biofilms of *P. fluorescens* were obtained in an ATR flow cell enclosed in an open circuit as described in a previous work [34]. In the present study, a ZnSe crystal was used, and the medium for biofilm initiation was LB/100. Briefly, a *P. fluorescens* suspension with $OD_{620} = 0.28$ ($\approx 10^8$ CFU/mL) in LB/100 was pumped into the ATR flow cell at a constant rate (42 mL/h) during 3 h to promote bacterial adhesion, and then the bacterial suspension was replaced by sterile LB/100 medium flow for 3 h at the same rate, obtaining a 6 h-old biofilm.

2.5. S4 (1–16)M4Ka action on the 6 h-old biofilm of P. fluorescens

The 6 h-old *P. fluorescens* biofilms were exposed for 24 h to either LB/100 medium, as the control experiment, or at three concentrations (MIC, 4xMIC, and 32xMIC) of peptide S4(1–16)M4Ka in sterile LB/100 medium. The pH of all the solutions was 7.0 ± 0.1. The peptide solutions were limpid, suggesting that the aggregation is negligible at the concentrations used [14,54]. For this, 40 mL of the sterile LB/100 medium solution, with or without AMP, was injected in the flow cell into a new closed circuit in maintaining the same flow rate as in previous both steps. The inoculation of the LB/100 medium and the peptide solutions were carefully performed under sterile conditions, avoiding formation of air bubbles in the flow cell. An abiotic experiment was conducted with the same conditions for a peptide solution at 4xMIC, i.e. sterile LB/100 medium was flowed in the flow cell during 6 h in the open circuit, followed by the flow of the peptide solution during 24 h in the closed circuit. Two independently conducted measurements were performed for every experiment, and they were consistent.

2.6. ATR–FTIR spectroscopy

The ATR–FTIR fingerprints of bacteria were monitored *in situ* and in real time during the development of the biofilms with or without the AMP. The ATR–FTIR spectra were recorded between 4000 and 800 cm^{-1} on a Bruker Vector 22 spectrometer equipped with a KBr beam splitter and a deuterated triglycine sulphate (DTGS) thermal detector. Spectra recording and data processing were performed using the Bruker OPUS 3.1 software. The resolution of the single beam spectra was 4 cm^{-1}. One hundred scans were collected per spectrum (corresponding to a 1-min accumulation time). All interferograms were Fourier processed using the Mertz phase correction mode and a Blackman-Harris three-term apodization function. No ATR correction was performed. ATR–FTIR spectra are shown with an absorbance scale corresponding to $\log(R_{reference}/R_{sample})$, where R is the internal reflectance of the device. A sample-reference spectrum acquired immediately before the step under study was recorded. Water vapour subtraction was performed. All spectra were baseline corrected at 3580, 2750, 1800, and 900 cm^{-1}. FTIR measurements were performed at 21 ± 1 °C in an air-conditioned room. For the biofilm monitoring, an ATR–FTIR flow cell (SPECAC) enclosing a trapezoidal ZnSe crystal with an incidence angle of 45° yielding six internal reflections on the upper face in contact with the sample. In the course of biofilm monitoring experiments, ATR–FTIR spectra were recorded every 10 min during the 6 h of bacterial inoculation and LB/100 circulation (open-circuit), then every 15 or 20 min during the 24 h of the peptide circulation (closed-circuit).

2.7. Fluorescence optical microscopy

Biofilms at the end of the experiments were analysed by fluorescence microscopy using the *Bac*Light™ stain kit (L7012, Molecular Probes, Eugene, USA) in order to determine the permeability of the sessile cells and the average bacterial surface coverage in the absence and presence of the AMP. This kit contains two nucleic acids stains: SYTO 9 (excitation/emission maxima: 480/500 nm) that penetrates all the cells, and propidium iodide that penetrates only cells with damaged membranes (excitation/emission maxima: 490/635 nm). Therefore, bacteria with intact membranes fluoresce green, while bacteria with damaged membranes fluoresce red. The ATR cell was demounted; the ZnSe crystal was carefully removed, rinsed with non-pyrogenic sterile water to remove non-adherent cells. The *Bac*Light™ solution was laid on the ZnSe crystal, and stained for 20 min in the dark at 21 ± 1 °C. The ZnSe crystal was then rinsed with non-pyrogenic sterile water to eliminate excess *Bac*Light™ solution, and wicked dry with a filter paper to remove excess water. The sample was mounted in *Bac*Light™ mounting oil as described by the instructions provided by the manufacturer. Both fluorescences were viewed simultaneously with the 100 x oil immersion objective of an Olympus BX51 microscope equipped with an Olympus XC50 camera.

2.8. AFM imaging and force measurements

AFM experiments were carried out using a MFP3D-BIO instrument (Asylum Research Technology, Atomic Force F & E GmbH, Mannheim, Germany). Silicon nitride cantilevers of conical shape were purchased from Bruker (MLCT-AU, Bruker-nano AXS, Palaiseau, France). The spring constants of the cantilevers measured using the thermal noise method were found to be 0.020–0.024 nN/nm. Experiments were performed in PBS (pH = 7.4) at room temperature. AFM images were recorded at room temperature (20 °C) in contact mode and in aqueous medium. The applied force between the tip and the surface was carefully monitored and minimized at about 0.25 nN, and all images were collected with a resolution of 512 × 512 pixels and a scan rate of 1 Hz. The nano indentation method provides the Young's modulus calculated from the force curve vs. the indentation curve. Mechanical properties were obtained by recording a grid map of 32-by-32 force curves at different locations of the biofilm surface. The maximal loading force was 4 nN, the piezodrive was fixed to 2 μm and the approach rate was 1000 nm/s. The bacterial spring constant (k_{bact}) was determined from the slope of the linear portions of the raw deflection versus piezo displacement curves [55] according to: $k_{bact} = \frac{k_s \cdot s}{(1-s)}$ where s is the experimentally accessible slope of the compliance region reached for sufficiently large loading forces, and k_s is the cantilever spring constant. The histograms corresponding to the statistic distribution of Young modulus E were estimated from the analysis of the approach curves according to the Sneddon model [56]. In this model, loading force F is given by:

$$F = \frac{2E \cdot \mathrm{Tan}(\alpha)}{\pi(1-\nu^2)}\,\delta^2$$

Where α is the semi top angle of the tip, δ is the indentation depth, and ν is the Poisson coefficient. All the force volume images were analysed by mean of an automatic Matlab algorithm described elsewhere [57].

3. Results and discussion

The MIC for S4(1–16)M4Ka was 3.125 mg/L or 1.8 μM for planktonic *P. fluorescens* (Pf). It was in the range of those measured for other Gram negative bacteria [15,17].

In order to assess the effect of this AMP on the development of Pf in sessile form, a 6 h-old biofilm was exposed for 24 h either to LB/100 medium (control) or to an AMP solution in LB/100 at three different concentrations (MIC, 4xMIC, and 32xMIC). The 6 h-old biofilm was obtained in two steps in an open circuit. The first one was the inoculation in the flow cell of a Pf suspension during three hours to initiate the bacterial adhesion, and the second one was the flow of a sterile LB/100 nutritive medium during three others hours to promote the biofilm development.

The changes in the ATR–FTIR spectra over 6-h of the biofilm formation were in agreement with our previous studies [34] (Fig. S1 in Supplementary Material or SM). In short, during the bacterial inoculation, the intensity of the whole bacterial ATR–FTIR fingerprint increased reflecting the attachment and the colonization of bacteria on the crystal. Subsequently, during the second 3-h period, the intensity of all bands continued to increase but the nucleic acids polysaccharide region, between 1200 and 900 cm^{-1}, increased at a higher rate than the amide II band located around 1550 cm^{-1} mainly associated with proteins. This increase reflected the biofilm development, the bacterial cells dividing on, colonizing the ZnSe surface, and producing extracellular polymeric substances. This 6 h-old biofilm also consisted of a single layer of bacteria as confirmed by epifluorescence microscopy. Bacteria had an average diameter of about 0.7 μm for 2–3 μm long. The penetration depth is of about 0.95 and 1.33 μm at 1550 and 1000 cm^{-1}, respectively, in the conditions used. Consequently, assuming that bacteria are in close contact with the ATR crystal, the whole bacterial cell are analysed with ZnSe crystals.

3.1. Development of the 6 h-old P. fluorescens biofilm in LB/100 medium (control experiment)

The 6 h-old *P. fluorescens* biofilm was exposed for 24 h to the sterile LB/100 medium that was injected in the flow cell into a closed circuit in maintaining the same flow rate as in previous steps. Fig. 1a shows the ATR–FTIR spectra recorded during this step. The reference spectrum is the spectrum of the 6 h-old Pf biofilm on the ZnSe ATR crystal recorded just before supplying sterile LB/100. Hence, the spectra in Fig. 1 reflect only the time evolution of the cells attached on the ZnSe crystal in the 6 h-old biofilm. They showed that during two hours the bacterial growth occurred on the crystal with the high synthesis of proteins

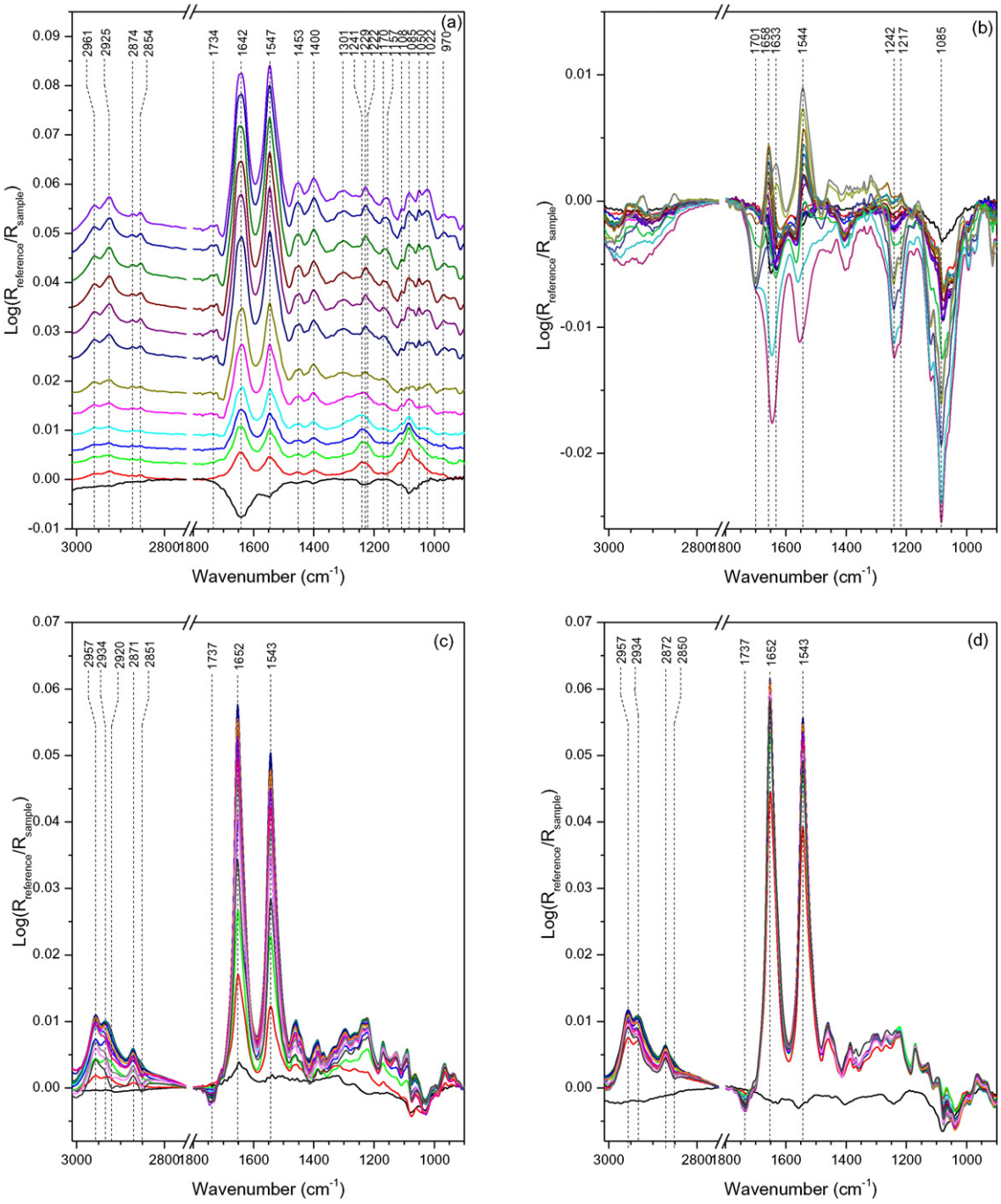

Fig. 1. Evolution over time of ATR–FTIR spectra from 6 to 30 h of the experiment during (a) the flow of sterile diluted 1:100 LB: 6, 7, 8, 9, 10, 11, 12, 15, 18, 21, 24, 27, and 30 h-old biofilm from the bottom to the top; (b-c) the flow of the solutions of the antimicrobial peptide in sterile diluted 1:100 LB at (b) 3.25 mg/L (MIC), (c) 12.5 mg/L (4xMIC) and (d) 100 mg/L (32xMIC): 6 h 15, 6 h 30, 6 h 45, 7 h, 7 h 15, 7 h 30, 7 h 45, 8 h, 8 h 15, 8 h 30, 8 h 45, 9 h, 12 h, 15 h, 18 h, 21 h, 24 h, 27 h, and 30 h-old biofilm. The background spectrum is the spectrum of the 6 h-old reference biofilm on the ZnSe ATR crystal. Times offset of spectra are used for clarity in Fig. 1(a).

(amide I and II bands at 1642 and 1547 cm^{-1}, respectively), nucleic acids and polysaccharides (region between 1250 and 1000 cm^{-1}). After this time, whereas amide bands continued to grow, nucleic acids bands decreased gradually (~1230, 1116, 1085 and 1042 cm^{-1}), and polysaccharidic bands (mainly at 1157, 1082, 1050 and 1022 cm^{-1} that were assigned to glycogen) grew from about 12 h to the end of the experiment as it was already observed in other conditions [35]. Of note, the first negative spectrum is due to the detachment of some bacteria due to a little air bubble generated when the tubes of the system were replaced. The 30 h-old biofilm was stained with the *Bac*light™ kit. A representative picture is given in Fig. 2a. The fluorescence of the bacteria was green showing intact membranes. In addition, a very high coverage was observed, and bacteria were arranged in multilayers. The infrared and fluorescence data showed the growth of a biofilm, however, the closed circulation of the nutritive medium changed the infrared spectral evolution of the biofilm with respect to open circuit conditions already used (Fig. S2 in SM) [35].

3.2. Development of the 6 h-old Pf biofilm exposed to the flow of solutions of peptide S4(1–16)M4Ka at 4xMIC and 32xMIC in LB/100 medium

As shown in Fig. 1c and 1d, the spectral evolution was totally different when the 6-h biofilm was exposed to the flow of solutions of peptide S4(1–16)M4Ka at 4xMIC or 32xMIC.

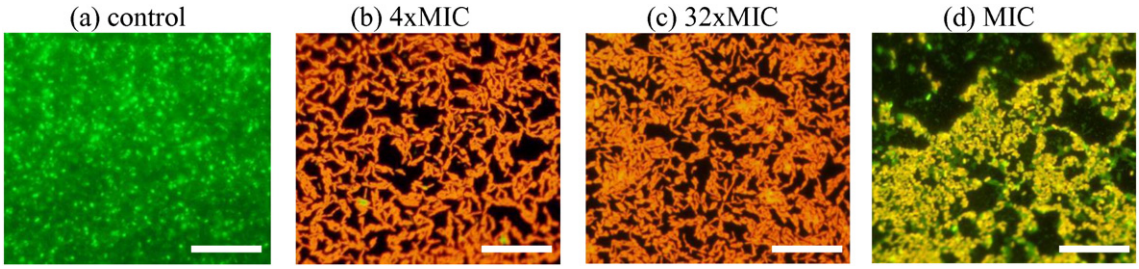

Fig. 2. Representative fluorescence microscopy images of *P. fluorescens* biofilms on the ZnSe crystal after 24 h of continuous flow on the 6 h-old biofilm of (a) sterile diluted 1:100 LB without peptide (control); (b, c, d) solutions of antimicrobial peptide at 12.5 mg/L (4xMIC), 100 mg/L (32xMIC), and 3.25 mg/L (MIC) in sterile diluted 1:100 LB, respectively. Bacteria were stained with the *Bac*light™ kit. Bar: 20 μm.

The presence of the AMP induced a very strong increase of the intensity of both the amide I and amide II bands associated with proteins at 1653 and 1644 cm^{-1}, respectively. When the same experiment was carried out without bacteria such an increase of both the amide I and amide II bands was not observed. The spectra exhibited only a weak signal in this region (Fig. 3a) reflecting a low quantity of AMP onto the crystal surface despite the high potential for adsorption of proteins on surfaces [58]. The spectral profile in region 2800–3000 cm^{-1} (C—H stretching's region) was also very different from the one observed during the initial bacterial colonization. Four bands at 2961, 2925, 2874 and 2854 cm^{-1} were observed during the elaboration of the 6 h-old biofilm. Only three quite intense main bands at 2957, 2934, and 2871 cm^{-1} occurred when the solution of AMP was flowed. The feature of these three bands fitted well with the one usually observed for proteins [59].

The maximum value of the integrated intensities of the amide II band is reached after one hour of circulation of the AMP at concentration 32xMIC whereas it took about 2 h 45 at concentration 4xMIC (Fig. 4a). Anyway, the maximum amide II value of the integrated intensities was the same for both experiments. The integrated intensities of amide II band decreased very slightly for the experiment at 32xMIC, whereas

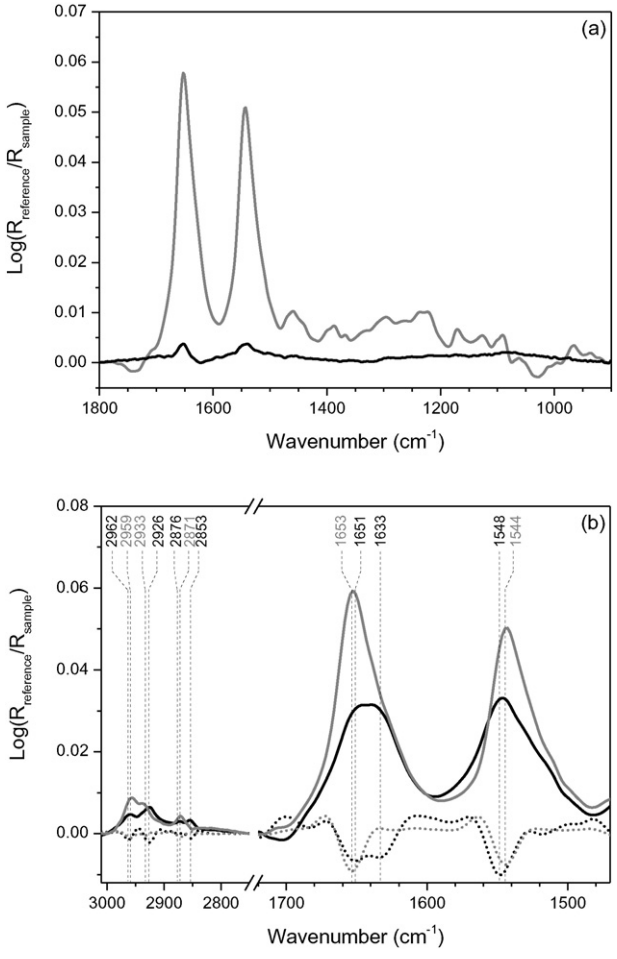

Fig. 3. Comparison of ATR–FTIR spectra (a) at 4 h of flow of solutions of the antimicrobial peptide in sterile diluted 1:100 LB at 12.5 mg/L (4xMIC) in absence of biofilm (black line) and in presence of the 6 h-old biofilm (grey line); (b) of 30 h-old biofilms in sterile diluted 1:100 LB without the antimicrobial peptide (black line), and in sterile diluted 1:100 LB with the antimicrobial peptide at 100 mg/L (32xMIC, grey line). The second derivative spectra are given in the dotted lines. The background spectrum is the spectrum of the 6 h-old reference biofilm on the ZnSe ATR crystal.

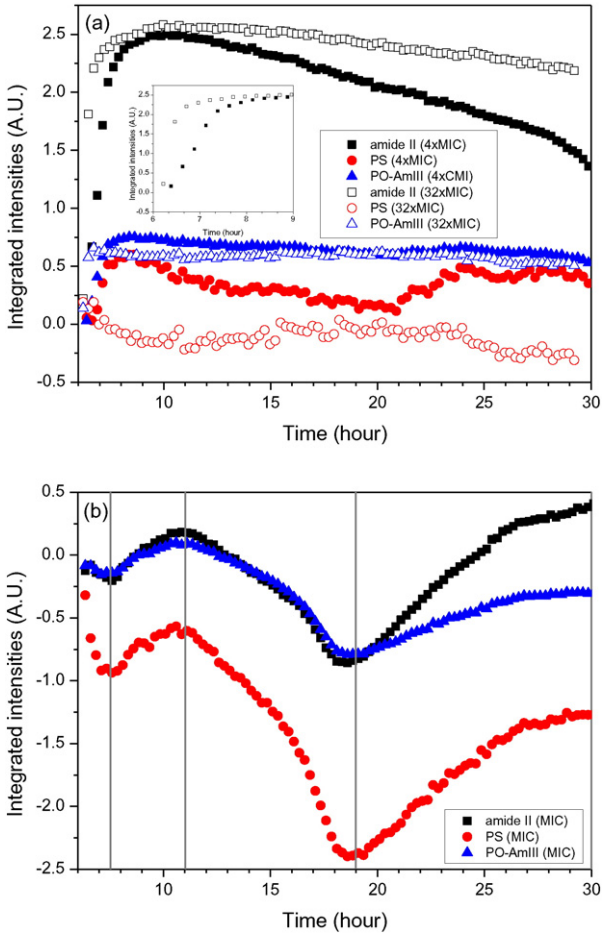

Fig. 4. Plot of integrated intensities as a function of time during the circulation of the antimicrobial peptide (a) at 12.5 mg/L (4xMIC, closed symbols) and 100 mg/L (32xMIC, open symbols). Insert: zoom from 6 to 9 h for the amide II bands; (b) 3.25 mg/L (MIC). Grey vertical lines: times corresponding to spectra used to calculate the difference spectra of Fig. 8. The background spectrum is the spectrum of the 6 h-old reference biofilm on the ZnSe ATR crystal. Key: amide II: amide II band (region 1597–1483 cm^{-1}); PO-AmIII: PO antisymmetric stretching and amide III band (region 1280–1188 cm^{-1}); PS: mainly C—C, C—O, PO stretchings (region 1187–952 cm^{-1}).

they significantly decreased for the experiment at 4xMIC from about 5 h of the circulation of the AMP (i.e. from the 11 h-old biofilm, Fig. 4a).

The fluorescence images of biofilms after 24 h exposure to the AMP stained with the *Bac*Light™ kit showed clearly bacteria in a monolayer where 100% of bacterial membranes were damaged (Fig. 2b-c). The average surface coverage was estimated to 35 ± 11% and 38 ± 8% for the experiments at 4xMIC and 32xMIC, respectively. These values were very similar to those obtained with the 6 h-old biofilm. It should be noted that although the membranes were damaged the cells were not deformed. These results suggested that when the 6-h biofilm was exposed to the AMP, the changes in ATR–FTIR spectra reflected a very high uptake of the AMP by sessile bacteria, and probably a high adsorption of the AMP on the bacterial membranes. Indeed, it is known that high AMP concentrations can be expected in the bacterial membranes [60]. This fact is also supported by the profile and the wavenumbers of the amide bands which were different from those observed in the case of the spectra recorded for the biofilms grown without AMP (Fig. 3b and S3 in SM), and were characteristic of an α-helical conformation [23]. Such a structure is adopted by this peptide family to form amphipathic structures allowing them to insert the hydrophobic face into the lipid bilayers [6,7,14].

Little and undefined variation was observed in the spectra below 1200 cm^{-1}. In particular, almost no change in the nucleic acids infrared fingerprint suggested a very rapid inhibition of nucleic acids biosynthesis upon the AMP treatment. The bacteria are stopped in proliferation and appeared to be trapped in the process of cell division. This result was in accordance with epifluorescence images that shown the same surface coverage by bacteria for the 6 h-old and these 30 h-old biofilms. In contrast, bands at 2920, 2851 and 1737 cm^{-1} decreased gradually during about the first 13 h of circulation of the AMP. These bands were assigned to lipids (mainly phospholipids and lipopolysaccharides (LPS) from the bacterial membrane) even though it was difficult to ascertain the decrease of phosphate bands around 1230 and 1085 cm^{-1} because of numerous overlapping bands in this region [59]. This decrease in intensity may reflect a slight loss of membrane lipids (likely LPS which are the major components of the outer leaflet [61,62]) from the sessile bacteria upon the AMP action.

All these findings, namely, a slight loss of some bacterial lipids, α-helical structure of the AMP, permeation of membranes, are quite consistent with the first stages of the accepted model which describes the mode of action of most AMPs against Gram-negative bacteria as follows [6,9,10,63,64]: the cationic AMPs are first attracted to negative bacterial surfaces, interact with the lipopolysaccharides on the outer leaflet, and pass through it. Once the cytoplasmic membrane is reached, peptides interact with the negatively charged phospholipid head groups. Insertion of the AMP into the outer leaflet leads to a disturbance of the outer membrane and permeabilizes this membrane to other peptide molecules in a process termed “self-promoted uptake” [9]. The peptide can move to the cytoplasm membrane by assuming an amphipathic α-helical conformation that allows them to insert the hydrophobic face into the bilayer. Then the membrane permeation occurs *via* one of the three general mechanisms named “barrel-stave pores”, “toroidal pores”, and “carpet” forming possibly transient pores or holes, and/or the AMP translocates across the membrane into the cytoplasm where they can interfere with essential intracellular processes [6,7,10]. It should be noted that these models of membrane permeation rely mainly on studies with model membranes and not studies in vivo like here. Furthermore, the latter stage is still widely debated. For dermaseptins, some studies suggested that at high concentration, they disrupt the bacterial membranes in a detergent-like manner (“carpet model”), leading to cellular lysis [7,64]. Others studies showed that some dermaseptins can also inhibit intracellular functions without damaging the cytoplasmic membrane at concentrations up to fivefold its MIC [65]. In the present study, although a slight loss of lipids and membrane permeation were observed, the fluorescence images did not show deformed cells and the IR–ATR spectra did not revealed a significant loss of sessile bacteria. To analyse more precisely injury of cell membranes upon AMP treatments, AFM studies were carried out.

Fig. 5 shows the AFM images and height cross sections obtained from the 6 h-old biofilm, and the 30 h-old biofilms after 24 h exposure to solutions of AMP at 4xMIC and 32xMIC. The 6 h-old biofilm was chosen for the blank biofilm because it was mainly a monolayer of bacteria as it was for the 30 h-old biofilms submitted to the solutions of AMP. The images recorded after slight N_2 drying of the biofilms did not give evidence of the occurrence of holes in the bacterial membrane. By this N_2 drying, the bacteria were flattened with an average height of about 200 and 125 nm for bacteria before and after treatment with the AMP at 4xMIC, respectively.

Such a flattening is generally observed when bacteria lose their intracellular water. Indeed, in hydrated medium the average diameter of untreated cells is around 600–700 nm [66]. The slight drying reduced by factors 3 and 5 the thickness of the bacteria for the untreated and the 4xMIC treated cells, respectively, which point out the antimicrobial effect of the peptide on the membrane permeability. Astonishingly, the flattening effect was less drastic when the AMP concentration was 32xMIC, since the same drying resulted in an average thickness of bacteria around 400 nm. The permeability of the bacterial membranes being intimately related to their nanomechanical properties, the AMP activity against the bacteria can be investigated through the elastic features of the bacterial cell wall by force spectroscopy.

Force-distance curves were recorded in aqueous medium, converted into force-indentation curves, and then analysed using the Sneddon model to generate statistical distributions of the Young modulus. Fig. 6 shows two types of histograms and typical force-indentation curves recorded on the biofilm and on the ZnSe crystal. Most curves were well-described by the Sneddon model, allowing us to obtain Young modulus values. The curves recorded before the action of the AMP against the bacteria in the 6 h-old biofilm yielded a pseudo Gaussian behaviour of the Young modulus distribution with an average value of 273 ± 81 kPa (which corresponds to an estimated bacterial spring constant of 0.018 nN/nm). This value was in the same range than the one measured on the planktonic form [66].

The statistical analysis of the bacterial elasticity in the 30 h-old biofilm with the flow of the AMP at 4xMIC (Fig. 6b) evidenced a lower Young modulus with an average value of 218 ± 58 kPa (estimated bacterial spring constant of 0.015 nN/nm). The distribution of the Young modulus of the bacterial cells in the 30 h-old biofilm with the flow of the AMP at 32xMIC was broad and mainly above 450 kPa, but by using a theoretical log normal fitting the most probable Young modulus was found at 772 ± 221 kPa (Fig. 6c, which corresponds to an estimated bacterial spring constant of 0.061 nN/nm). These results are consistent with those above regarding the effect of a slight N_2 drying of the biofilms. The sessile cells exposed to the AMP at 4xMIC were less rigid and more permeable than the untreated cells. This result is in good agreement with IR–ATR spectra that highlighted the loss of some membrane lipids as well as of a part of the AMP. The decrease of the cell wall stiffness upon antimicrobial treatment was already observed on *Staphylococcus aureus* treated with lysostaphin where the Young modulus was reduced by a factor 9. On the contrary, the sessile cells exposed to the AMP at 32xMIC were less permeable and more rigid than the untreated cells. Such a stiffening effect was already reported for *P. aeruginosa* treated with colistin (from 0.33 to 0.75 nN/nm, before and after treatment, respectively) [67]. The authors suggested that this increase of the permeability goes in pair with an incorporation of colistin into the peptidoglycan layer. This discrepancy of effect between concentrations at 4xMIC and at 32xMIC was unexpected. To gain insights into the changes occurring at the highest concentration of AMP, the nanomechanical properties of the bacterial cells were monitored Throughout the AMP treatment. Fig. 7 compares the time-evolution of the average Young modulus with the kinetics of AMP adsorption through the integrated intensities of the amide II band, and the integrated intensities of the ester C═O stretching band from the

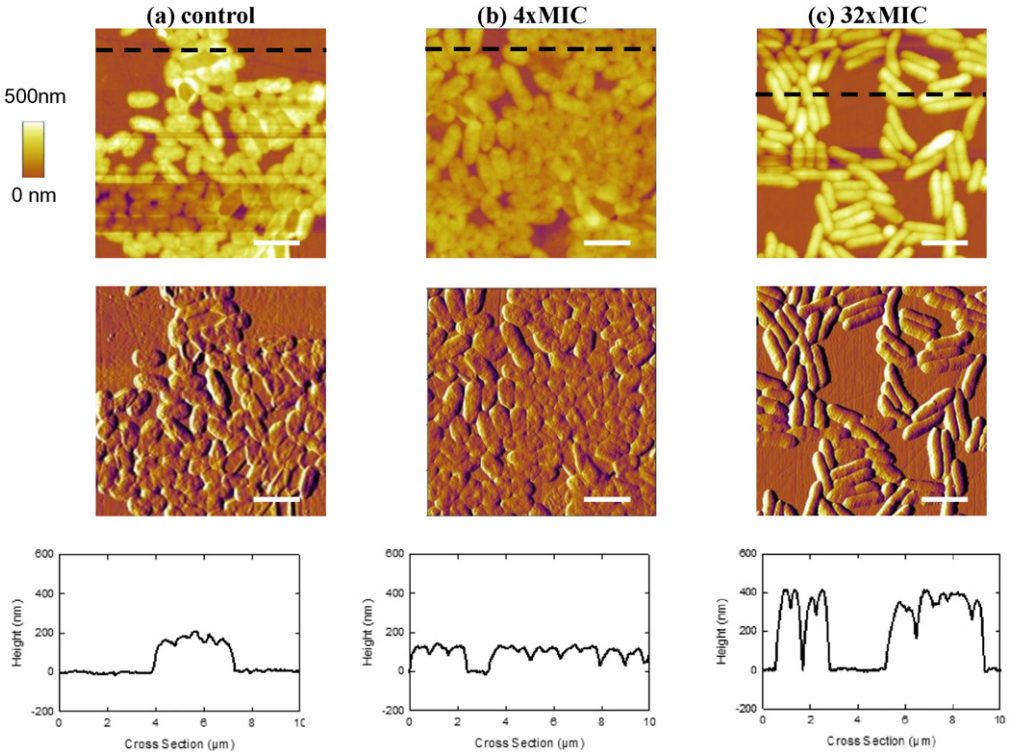

Fig. 5. Morphology of the biofilm before and after AMP treatment. Height images (top panel) and deflection images (middle panel) were recorded on (a) the 6 h-old biofilm, (b) the 30 h-old biofilm treated with the AMP at 12.5 mg/L (4xMIC), and (c) the 30 h-old biofilm treated with the AMP at 100 mg/L (32xMIC). The height profiles (bottom panel) correspond to the lateral cross sections indicated by the black dashed lines. Bar: 2 µm.

membrane lipids at 1737 cm^{-1}. The time evolution of the AMP effect can be divided into three phases: (i) In the first one, the Young modulus decreased during about one hour to reach a minimum value of 200 kPa at about 6 h 45 of the experiment. This value of the Young modulus was very similar to the one obtained at 4xMIC after 30 h of the experiment. During the same time the integrated intensities of the amide II band

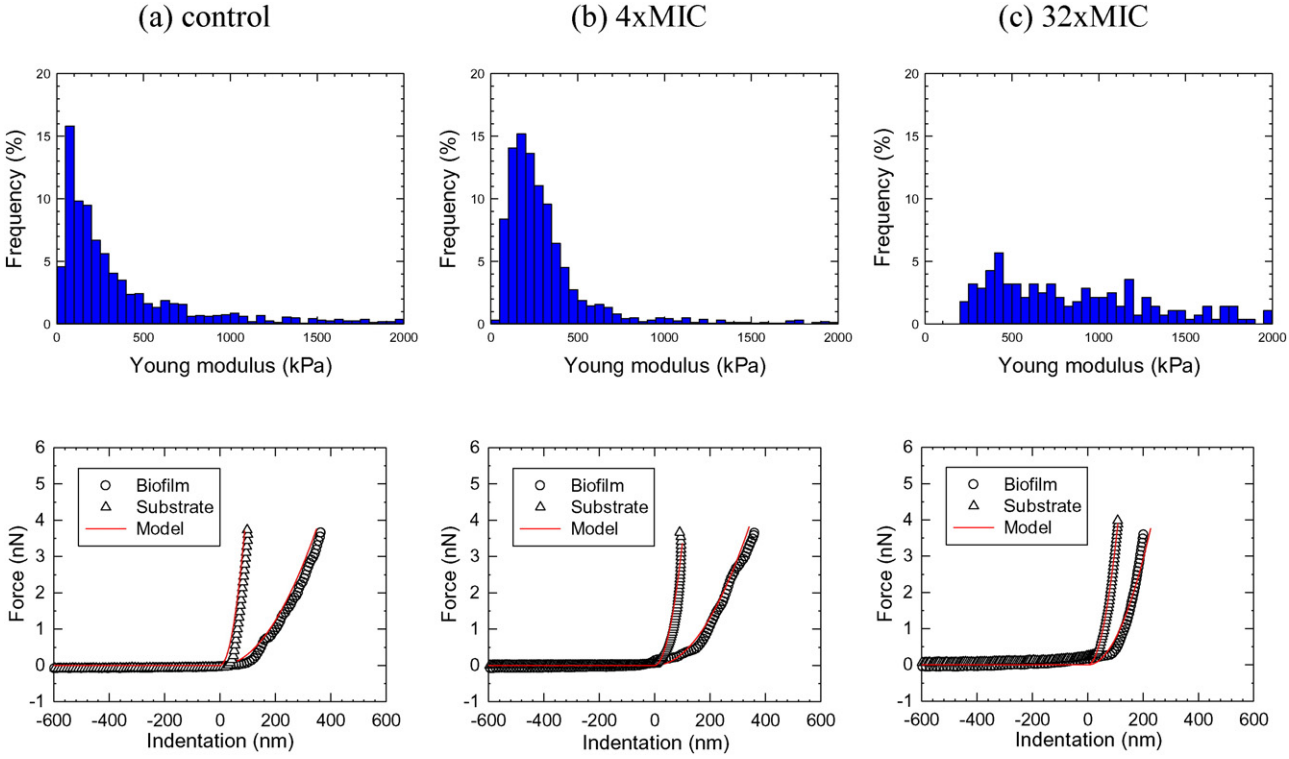

Fig. 6. Nanomechanical properties for *P. fluorescens* in PBS solution. Statistical distributions of the Young modulus, and representative force-indentation curves (open circle and triangle) with the theoretical model (red lines) taken from the biofilm and the substrate. Measurements were performed on (a) the 6 h-old biofilm, (b) the 30 h-old biofilm treated with the AMP at 12.5 mg/L (4xMIC), and (c) the 30 h-old biofilm treated with the AMP at 100 mg/L (32xMIC), respectively.

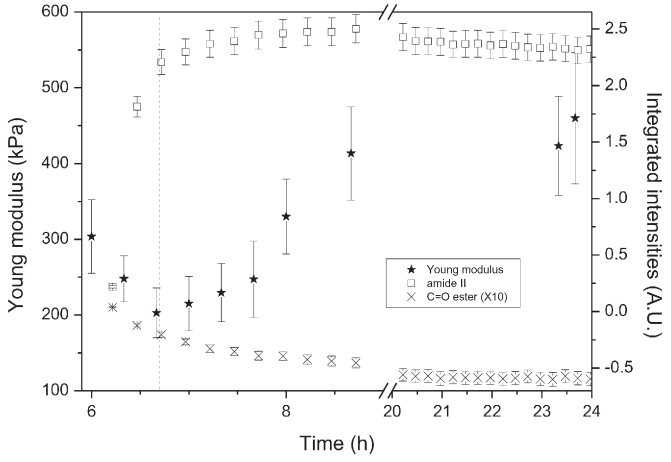

Fig. 7. Left scale: Plot as a function of time of the Young modulus (stars) of sessile bacteria treated with the AMP at 100 mg/L (32xMIC). Right scale: Plot as a function of time of the infrared integrated intensities during the treatment with the AMP at 100 mg/L (32xMIC). The background spectrum is the 6 h-old biofilm on the ZnSe ATR crystal. Key: amide II: amide II band (open squares, region 1597–1483 cm^{-1}); C═O ester: C═O stretching of phospholipids (crosses, region 1762–1719 cm^{-1}).

drastically increased whereas those of the ester C═O stretching band decreased gradually.

(ii) Then, in the second phase, both infrared integrated intensities continued their evolution more slightly during about 2 h. On the contrary, the Young modulus of the bacteria increased drastically. (iii) After 10 h of the experiment a steady state was reached for all the data measured (Fig. 7). The high adsorption of the AMP leading to the decrease of the Young modulus and a loss of membrane lipids in the first phase was probably connected to the degradation of the cell wall. The mechanism involved in this period of time should be the same as for the 4xMIC concentration. However, when a threshold concentration is reached at the 32xMIC concentration, another phenomenon occurred. It is suggested that the transient holes became plugged by the AMP at very high concentration leading to the accumulation of the AMP in the cell wall concomitantly to the increase of the Young modulus. These results suggested that when the sorption of the AMP reached a maximum on the bacteria, the membrane lipid loss became negligible because of the very high insertion of the AMP in the cell wall structure. This explanation is corroborated by the structure in α-helix of the AMP that occurs only when it is associated to lipid bilayers (Fig. 1d) [14]. Infrared data showed almost no evolution of the bacterial metabolism during the flowing of the AMP (inhibition of the nucleic acid synthesis), it is suggested that something like a petrification was induced by the high concentration of the AMP. This effect may be due by an intracellular action of the peptide that inhibited further growth of the bacteria.

To sum up, it is proposed that the mechanism of action of S4(1–16)M4Ka followed at the beginning a 'carpet-like' model for the peptide sorption on the sessile bacteria involving a high local concentration on the surface of the membrane after all the surface of the membrane is covered with the AMP as it was already described for dermaseptin S and analogues [64]. However, the AMP action did not lead here to the lysis of the sessile bacteria. The AMP inhibited intracellular processes such as nucleic acids synthesis, suggesting that part of the peptide was translocated across the membrane in the bacterial cytoplasm.

3.3. Development of the 6 h-old Pf biofilm exposed to the flow of a solution of peptide S4(1–16)M4Ka at the MIC in LB/100 medium

When the 6-h biofilm was exposed to a flow of a solution of the AMP at the MIC, the spectral evolution over time was very different from the two other series (Fig. 2b-d). It exhibited four different periods as it is shown by the evolution of the band integrated intensities as a function of the time (Fig. 4b). Fig. 8 shows the difference spectra calculated from the border times of these four periods. The first period (from 6 h to 7 h 30) corresponded to the detachment of some biomass, but also to the beginning of the sorption of the AMP on the bacteria. These facts are supported by the negative bands in regions 1650–1550 cm^{-1} (amide I and II bands of bacterial proteins) and 1100–1000 cm^{-1} (polysaccharides and nucleic acids region), and by the appearance of positive bands at 1653 and 1540 cm^{-1}, the latter couple being assigned to the amide I and II bands of the AMP with an α-helix conformation (Fig. 8a). In the second period (from 7 h 30 to 11 h), those amide I and II bands continued to increase. The sorption of the AMP on the bacteria continued (Figs. 4b and 8b). No inhibition of the biosynthesis nucleic acids was observed during this period, since the bands centred at 1230 and 1084 cm^{-1}, assigned principally to nucleic acids, increased in the spectra (Fig. 8b). A significant loss of biomass was observed during the third period of time (from 11 h to 19 h, Figs. 4b and 8c). Notably, the amide I and II bands at 1653 and 1540 cm^{-1}, as well as the C—H stretching bands at 2957, 2935 and 2874 cm^{-1} decreased drastically. These bands were already observed for the other experiments at higher concentrations of AMP, and assigned to the AMP in α-helix conformation. As it was observed for the experiment at 4xMIC, a high desorption of the AMP occurred from about 11 h. It was not the case for the experiment at 32xMIC where the AMP was in large excess. The negative bands at 1703, 1240, 1222, 1118, 1085, 1060 cm^{-1} (Fig. 8c) are assigned to nucleic acids [59].

This loss of metabolic activity could be due to the onset of antimicrobial activity of peptide when a critical concentration is reached [14]. From 19 h, all the integrated intensities increased (Fig. 4b). The difference spectrum obtained by the subtraction of the spectrum of the 19 h-old biofilm from the spectrum of the 30 h-old biofilm showed the characteristic features of Pf (Fig. 8d). Indeed four C—H stretching bands (2957, 2923, 2874, and 2853 cm^{-1}), amide I and II bands at 1642 and 1540 cm^{-1}, and bands assigned to nucleic acids at 1230 and 1084 cm^{-1} were typical of Pf that grew as a biofilm associated with the production of glycogen as it is indicated by the increase of bands at 1154, 1054 and 1027 cm^{-1} (Fig. 8d) [35].

The fluorescence pictures of the 30 h-old biofilm stained with the *Bac*light™ kit were in good agreement with these conclusions (Fig. 2d). They showed a heterogeneous layer of biofilm with damaged bacteria (orange in the picture), live bacteria (green in the picture) and cell fragments (size often smaller than a bacterium, and with an undefined form, usually with dark green fluorescence). Unfortunately, these

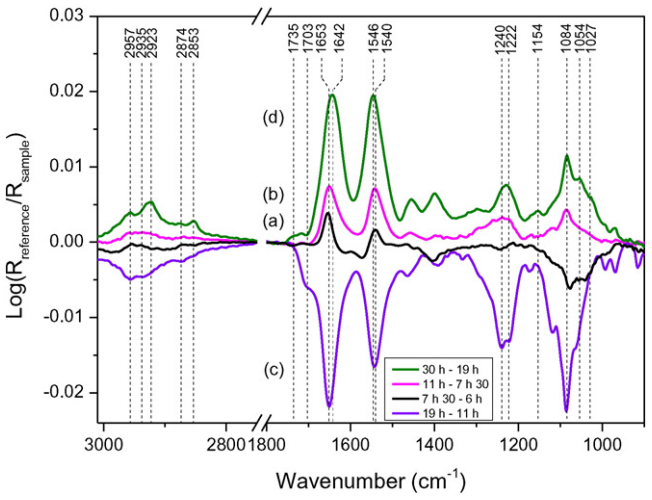

Fig. 8. Differences of ATR-FTIR spectra recorded during flow of the solution of the antimicrobial peptide in sterile diluted 1:100 LB at 3.25 mg/L (MIC). (a) Spectrum 7 h 30 old biofilm − 6 h old biofilm (black) (b) spectrum 11 h old biofilm − 7 h 30 old biofilm (magenta), (c) spectrum 19 h old biofilm − 11 h old biofilm (violet), (d) spectrum 30 h old biofilm − 19 h old biofilm (green).

features did not allow the measurement of reliable AFM images and *a fortiori* nano indentation with force spectroscopy experiments.

4. Conclusion

The present work shows clearly that the ATR–FTIR technique can be used to probe and *in situ* monitor, at the molecular scale and in real time, the biochemical changes induced by AMPs in sessile bacteria cells over the first stages of biofilm formation. However, this technique does not analyse one single cell but a large part of bacteria present on the crystal. The combination with atomic force microscopy gave information localized at the cellular scale the biochemical changes revealed in the ATR–FTIR spectra. Consequently, they can be valuable tools to increase our understanding about modes of action of AMPs on sessile bacteria, and to optimize their structure in order to improve their antimicrobial activity and toxicity profile. The response of the 6-h biofilm exposed to the AMP depends strongly on the concentration of the AMP. The tested peptide at concentration 12.5 mg/L (or 7.2 μM), which stayed in the range of usual MIC of AMP for planktonic bacteria, exhibited an inhibitory activity against the development of a mature biofilm. It is important for the preventing formation of biofilm, because once the early biofilm is inhibited, the mature biofilm may in turn be prevented or at least controlled.

Conflict of interest

All authors declare no conflict of interest including any financial, personal or other relationships with other people or organizations within three years of beginning the submitted work that could inappropriately influence, or be perceived to influence, their work.

Acknowledgements

The authors warmly thank Pr Khaled Hani (Laboratoire de Biochimie, Faculté de Médecine de Sousse, Avenue Mohamed Karoui — 4002 Sousse, Tunisie) for allowing S. Saadi to come at LCPME, and for the purchase of the antimicrobial peptide.

Appendix A. Supplementary data

Supplementary data to this article can be found online at http://dx.doi.org/10.1016/j.bbamem.2015.10.015.

References

[1] R.M. Donlan, J.W. Costerton, Biofilms: survival mechanisms of clinically relevant microorganisms, Clin. Microbiol. Rev. 15 (2002) 167.
[2] A. Bridier, R. Briandet, V. Thomas, F. Dubois-Brissonnet, Resistance of bacterial biofilms to disinfectants: a review, Biofouling 27 (2011) 1017.
[3] H. Ceri, M.E. Olson, C. Stremick, R.R. Read, D. Morck, A. Buret, The Calgary biofilm device: new technology for rapid determination of antibiotic susceptibilities of bacterial biofilms, J. Clin. Microbiol. 37 (2014) 1771.
[4] P.S. Stewart, Mechanisms of antibiotic resistance in bacterial biofilms, Int. J. Med. Microbiol. 292 (2002) 107.
[5] R. Nuri, T. Shprung, Y. Shai, Defensive remodeling: How bacterial surface properties and biofilm formation promote resistance to antimicrobial peptides, Biochim. Biophys, Acta, Biomembr. 1848 (2015) 3089.
[6] A. Tossi, L. Sandri, A. Giangaspero, Amphipathic, α-helical antimicrobial peptides, Biopolymers (Peptide Science) 55 (2000) 4.
[7] Y. Shai, Mode of action of membrane active antimicrobial peptides, Biopolymers (Peptide Science) 66 (2002) 236.
[8] M.R. Yeaman, N.Y. Yount, Mechanisms of antimicrobial peptide action and resistance, Pharmacol. Rev. 55 (2003) 27.
[9] H. Jenssen, P. Hamill, R.E.W. Hancock, Peptide antimicrobial agents, Clin. Microbiol. Rev. 19 (2006) 491.
[10] K.A. Brogden, Antimicrobial peptides: pore formers or metabolic inhibitors in bacteria? Nat. Rev. Microbiol. 3 (2005) 238.
[11] P. Nicolas, C. El Amri, The dermaseptin superfamily: a gene-based combinatorial library of antimicrobial peptides, Biochim. Biophys. Acta Biomembr. 1788 (2009) 1537.
[12] A. Mor, V.H. Nguyen, A. Delfour, D. Migliore-Samour, P. Nicolas, Isolation, amino acid sequence, and synthesis of dermaseptin, a novel antimicrobial peptide of amphibian skin, Biochem. 30 (1991) 8824.
[13] A. Mor, K. Hani, P. Nicolas, The vertebrate peptide antibiotics dermaseptins have overlapping structural features but target specific microorganisms, J. Biol. Chem. 269 (1994) 31635.
[14] I. Kustanovich, D.E. Shalev, M. Mikhlin, L. Gaidukov, A. Mor, Structural requirements for potent versus selective cytotoxicity for antimicrobial dermaseptin S4 derivatives, J. Biol. Chem. 277 (2002) 16941.
[15] A. Zairi, F. Tangy, S. Saadi, K. Hani, In vitro activity of dermaseptin S4 derivatives against genital infections pathogens, Regul. Toxicol. Pharmacol. 50 (2008) 353.
[16] C. Lorin, H. Saidi, A. Belaid, A. Zairi, F. Baleux, H. Hocini, L. Bélec, K. Hani, F. Tangy, The antimicrobial peptide dermaseptin S4 inhibits HIV-1 infectivity in vitro, Virology 334 (2005) 264.
[17] S. Navon-Venezia, R. Feder, L. Gaidukov, Y. Carmeli, A. Mor, Antibacterial properties of dermaseptin S4 derivatives with in vivo activity, Antimicrob. Agents Chemother. 46 (2002) 689.
[18] G.X. Wei, A.N. Campagna, L.A. Bobek, Effect of MUC7 peptides on the growth of bacteria and on *Streptococcus mutans* biofilm, J. Antimicrob. Chemother. 57 (2006) 1100.
[19] S. Hou, Z. Liu, A.W. Young, S.L. Mark, N.R. Kallenbach, D. Ren, Effects of Trp- and Arg-containing antimicrobial-peptide structure on inhibition of *Escherichia coli* planktonic growth and biofilm formation, Appl. Environ. Microbiol. 76 (2010) 1967.
[20] S.C. Park, Y. Park, K.S. Hahm, The role of antimicrobial peptides in preventing multidrug-resistant bacterial infections and biofilm formation, Int. J. Mol. Sci. 12 (2011) 5971.
[21] C. de la Fuente-Núñez, V. Korolik, M. Bains, U. Nguyen, E.B.M. Breidenstein, S. Horsman, S. Lewenza, L. Burrows, R.E.W. Hancock, Inhibition of bacterial biofilm formation and swarming motility by a small synthetic cationic peptide, Antimicrob. Agents Chemother. 56 (2012) 2696.
[22] W. Wang, R. Tao, Z. Tong, Y. Ding, R. Kuang, S. Zhai, J. Liu, L. Ni, Effect of a novel antimicrobial peptide chrysophsin-1 on oral pathogens and *Streptococcus mutans* biofilms, Peptides 33 (2012) 212.
[23] C. Nagant, B. Pitts, K. Nazmi, M. Vandenbranden, J.G. Bolscher, P.S. Stewart, J.P. Dehaye, Identification of peptides derived from the human antimicrobial peptide LL-37 active against biofilms formed by *Pseudomonas aeruginosa* using a library of truncated fragments, Antimicrob. Agents Chemother. 56 (2012) 5698.
[24] V. Luca, A. Stringaro, M. Colone, A. Pini, M.L. Mangoni, Esculentin(1–21), an amphibian skin membrane-active peptide with potent activity on both planktonic and biofilm cells of the bacterial pathogen *Pseudomonas aeruginosa*, Cell. Mol. Life Sci. 70 (2013) 2773.
[25] H. Li, J.W. Cheng, H.Y. Yu, Y. Xin, L. Tang, Y. Ma, Effect of the antimicrobial peptide D-Nal-Pac-525 on the growth of *Streptococcus mutans* and its biofilm formation, J. Microbiol. Biotechnol. 23 (2013) 1070.
[26] A. Almaaytah, S. Tarazi, F. Alsheyab, Q. Al-Balas, T. Mukattash, Antimicrobial and antibiofilm activity of mauriporin, a multifunctional scorpion venom peptide, Int. J. Pept. Res. Ther. 20 (2014) 397.
[27] A. Zairi, L. Ferrières, P. Latour-Lambert, C. Beloin, F. Tangy, J.M. Ghigo, K. Hani, *In vitro* activities of dermaseptins K4S4 and K4K20S4 against *Escherichia coli*, *Staphylococcus aureus*, and *Pseudomonas aeruginosa* planktonic growth and biofilm formation, Antimicrob. Agents Chemother. 58 (2014) 2221.
[28] T. Anunthawan, C. de la Fuente-Núñez, R.E.W. Hancock, S. Klaynongsruang, Cationic amphipathic peptides KT2 and RT2 are taken up into bacterial cells and kill planktonic and biofilm bacteria, Biochim. Biophys. Acta, Biomembr. 1848 (2015) 1352.
[29] E.C. López-Diez, C.L. Winder, L. Ashton, F. Currie, R. Goodacre, Monitoring the mode of action of antibiotics using Raman spectroscopy: investigating subinhibitory effects of amikacin on *Pseudomonas aeruginosa*, Anal. Chem. 77 (2005) 2901.
[30] X. Lu, B.A. Rasco, J.M.F. Jabal, D.E. Aston, M. Lin, M.E. Konkel, Investigating antibacterial effects of garlic (*Allium sativum*) concentrate and garlic-derived organosulfur compounds on *Campylobacter jejuni* by using Fourier transform infrared spectroscopy, Raman spectroscopy, and electron microscopy, Appl. Environ. Microbiol. 77 (2011) 5257.
[31] X. Lu, D.R. Samuelson, B.A. Rasco, M.E. Kondel, Antimicrobial effect of diallyl sulphide on *Campylobacter jejuni* biofilms, J. Antimicrob. Chemother. 67 (2012) 1915.
[32] T. Rema, J.R. Lawrence, J.J. Dynes, A.P. Hitchcock, D.R. Korber, Microscopic and spectroscopic analyses of chlorhexidine tolerance in *Delftia acidovorans* biofilms, Antimicrob. Agents Chemother. 58 (2014) 5673.
[33] S.Y. Kang, P.J. Bremer, K.W. Kim, A.J. McQuillan, Monitoring metal ion binding in single-layer *Pseudomonas aeruginosa* biofilms using ATR–IR spectroscopy, Langmuir 22 (2006) 286.
[34] F. Quilès, F. Humbert, A. Delille, Analysis of changes in attenuated total reflection FTIR fingerprints of *Pseudomonas fluorescens* from planktonic state to nascent biofilm state, Spectrochim. Acta A 75 (2010) 610.
[35] F. Quilès, F. Humbert, On the production of glycogen by *Pseudomonas fluorescens* during biofilm development: an in situ study by attenuated total reflection-infrared with chemometrics, Biofouling 30 (2014) 709.
[36] G.S. Lorite, A.A. de Sousa, D. Neubauer, B. Mizaikoff, C. Kranz, M.A. Cotta, On the role of extracellular polymeric substances during early stages of *Xylella fastidiosa* biofilm formation, Colloids Surf.,B 102 (2013) 519.
[37] P.A. Suci, M.W. Mittelman, F.P. Yu, G.G. Geesey, Investigation of ciprofloxacin penetration into *Pseudomonas aeruginosa* biofilms, Antimicrob. Agents Chemother. 38 (1994) 2125.
[38] P.A. Suci, J.D. Vrany, M.W. Mittelman, Investigation of interactions between antimicrobial agents and bacterial biofilms using attenuated total reflection Fourier transform infrared spectroscopy, Biomaterials 19 (1998) 327.
[39] G. Francius, S. Lebeer, D. Alsteens, L. Wildling, H.J. Gruber, P. Hols, S. De Keersmaecker, J. Vanderleyden, Y.F. Dufrêne, Detection, localization, and conformational analysis of single polysaccharide molecules on live bacteria, ACS Nano 2 (2008) 1921.
[40] G. André, M. Deghorain, P.A. Bron, I.I. van Swan, M. Kleerebezem, P. Hols, Y.F. Dufrêne, Fluorescence and atomic force microscopy imaging of wall teichoic acids in *Lactobacillus plantarum*, ACS Chem. Biol. 6 (2011) 366.

[41] Y.F. Dufrêne, Atomic force microscopy of fungal cell walls: an update, Yeast 27 (2010) 465.
[42] F. Gaboriaud, Y.F. Dufrêne, Atomic force microscopy of microbial cells: application to nanomechanical properties, surface forces and molecular recognition forces, Colloids Surf., B 54 (2007) 10.
[43] N. Jalili, K. Laxminarayana, A review of atomic force microscopy imaging systems: application to molecular metrology and biological sciences, Mechatronics 14 (2004) 907.
[44] I.M. Torcato, M.A.R.B. Castanho, S.T. Henriques, The application of biophysical techniques to study antimicrobial peptides, Spectrosc. Int. J. 27 (2012) 541.
[45] M. Radmacher, Measuring the Elastic Properties of Living Cells by the Atomic Force Microscope, Methods in Cell Biology, Elsevier, 2002 67–90.
[46] A. Engel, D.J. Müller, Observing single biomolecules at work with the atomic force microscope, Nat. Struct. Biol. 7 (2000) 715.
[47] Y.F. Dufrêne, Atomic force microscopy, a powerful tool in microbiology, J. Bacteriol. 184 (2002) 5205.
[48] M. Meincken, D.L. Holroyd, M. Rautenbach, Atomic force microscopy study of the effect of antimicrobial peptides on the cell envelope of *Escherichia coli*, Antimicrob. Agents Chemother. 49 (2005) 4085.
[49] G.E. Fantner, R.J. Barbero, D.S. Gray, A.M. Belcher, Kinetics of antimicrobial peptide activity measured on individual bacterial cells using high-speed atomic force microscopy, Nat. Nanotechnol. 5 (2010) 280.
[50] A. Zdybicka-Barabas, B. Januszanis, P. Mak, M. Cytrynska, An atomic force microscopy study of *Galleria mellonella* apolipophorin III effect on bacteria, Biochim. Biophys. Acta, Biomembr. 1808 (2011) 1896.
[51] T. Jacquet, C. Cailliez-Grimal, G. Francius, F. Borges, M. Imran, J.F.L. Duval, A.M. Revol-Junelles, Antibacterial activity of class IIa bacteriocin Cbn BM1 depends on the physiological state of the target bacteria, Res. Microbiol. 163 (2012) 323.
[52] S. Lu, G. Walters, R. Parg, J.R. Dutcher, Nanomechanical response of bacterial cells to cationic antimicrobial peptides, Soft Matter 10 (2014) 1806.
[53] A. Mularski, J.J. Wilksch, H. Wang, M.A. Hossain, J.D. Wade, F. Separovic, R.A. Strugnell, M.L. Gee, Atomic force microscopy reveals the mechanobiology of lytic peptide action on bacteria, Langmuir 31 (2015) 6164.
[54] R. Feder, R. Dagan, A. Mor, Structure-activity relationship study of antimicrobial dermaseptin S4 showing the consequences of peptide oligomerization on selective cytotoxicity, J. Biol. Chem. 275 (2000) 4230.
[55] A. Boulbitch, Deformation of the envelope of a spherical Gram-negative bacterium during the atomic force microscopic measurements, J. Electron Microsc. 49 (2000) 459.
[56] I.N. Sneddon, The relation between load and penetration in the axisymmetric Boussinesq problem for a punch of arbitrary profile, Int. J. Eng. Sci. 3 (1965) 47.
[57] P. Polyakov, C. Soussen, J. Duan, J.F.L. Duval, D. Brie, G. Francius, Automated force volume image processing for biological samples, PLoS One 6 (2011) e18887.
[58] K. Nakanishi, T. Sakiyama, K. Imamura, On the adsorption of proteins on solid surfaces, a common but very complicated phenomenon, J. Biosci. Bioeng. 91 (2001) 233.
[59] D. Naumann, FT-infrared and FT-Raman spectroscopy in biological research, in: H.U. Gremlich, B. Yan (Eds.), Infrared and Raman spectroscopy of biological materials, Practical Spectroscopy Series, 24, Marcel Dekker, Inc., New York 2001, pp. 323–377.
[60] M.N. Melo, R. Ferre, A.R.B. Castanho, Antimicrobial peptides: linking partition, activity and high membrane-bound concentrations, Nat. Rev. Microbiol. 7 (2009) 245.
[61] C. Alexander, E.T. Rietschel, Bacterial lipopolysaccharides and innate immunity, J. Endotoxin Res. 7 (2001) 167.
[62] N. Papo, Y. Shai, A molecular mechanism for lipopolysaccharide protection of Gram-negative bacteria from antimicrobial peptides, J. Biol. Chem. 280 (2005) 10378.
[63] M. Zasloff, Antimicrobial peptides of multicellular organisms, Nature 415 (2002) 389.
[64] Y. Shai, Mechanism of the binding, insertion and destabilization of phospholipid bilayer membranes by α-helical antimicrobial and cell non-selective membrane-lytic peptides, Biochim. Biophys. Acta, Biomembr. 1462 (1999) 55.
[65] A. Patrzykat, C.L. Friedrich, L. Zhang, V. Mendoza, R.E.W. Hancock, Sublethal concentrations of pleurocidin-derived antimicrobial peptides inhibit macromolecular synthesis in *Escherichia coli*, Antimicrob. Agents Chemother. 46 (2002) 605.
[66] F. Quilès, P. Polyakov, F. Humbert, G. Francius, Production of extracellular glycogen by *Pseudomonas fluorescens*: spectroscopic evidence and conformational analysis by biomolecular recognition, Biomacromolecules 13 (2012) 2118.
[67] N.P. Mortensen, J.D. Fowlkes, C.J. Sullivan, D.P. Allison, N.B. Larsen, S. Molin, M.J. Doktycz, Effects of colistin on surface ultrastructure and nanomechanics of *Pseudomonas aeruginosa* cells, Langmuir 25 (2009) 3728.